Precambrian Research 309 (2018) 88–101

Contents lists available at ScienceDirect

Precambrian Research

journal homepage: www.elsevier.com/locate/precamres

Formation of the Neoproterozoic ophiolites in southern China: New constraints from trace element and PGE geochemistry and Os isotopes

Zi-Ming Sun[a], Xiao-Lei Wang[a,*], Liang Qi[b], Feng-Feng Zhang[a], Di Wang[a], Jun-Yong Li[a], Ming-Gang Yu[c], Xu-Jie Shu[a,c]

[a] State Key Laboratory for Mineral Deposits Research, School of Earth Sciences and Engineering, Nanjing University, Nanjing 210046, China
[b] State Key Laboratory of Ore Deposit Geochemistry, Institute of Geochemistry, Chinese Academy of Sciences, Guiyang 550081, China
[c] Nanjing Institute of Geology and Mineral Resources, Nanjing 210016, China

ARTICLE INFO

Keywords:
South Anhui ophiolite
Northeast Jiangxi ophiolite
Jiangnan Orogen
Os isotopes
Platinum group elements

ABSTRACT

The South Anhui ophiolite (SAO) and the Northeast Jiangxi ophiolite (NJO) are the only two known Precambrian ophiolite suites within the eastern segment of the Jiangnan Orogen, South China. These ophiolites may provide significant insights into the convergence history of the South China Block during the Rodinia supercontinent cycle. SHRIMP zircon U–Pb dating indicates that the SAO formed at 831 ± 5 Ma whereas the NJO formed at ca. 1000 Ma. Modal mineral assemblages and the preservation of relict primary mineral assemblages indicate that serpentinized peridotites from both ophiolites were mainly harzburgite in protolith. Relict olivine and orthopyroxene fragments within both ophiolite suites yield similarly high Mg# values. The serpentinized peridotite samples yield U-shaped rare earth element patterns and contain high-Cr# spinel, both of which are indicative of supra-subduction zone ophiolites. However, serpentinized peridotites within the SAO contain olivine and clinopyroxene with slightly higher Mg# values, and have lower platinum-group element (PGE) and trace element concentrations than peridotites from the NJO. The SAO peridotites are also depleted in Ir, Pt, and Pd, in contrast to the flat and chondrite-like PGE patterns of the NJO peridotites. These observations indicate that compared with the NJO, SAO peridotites were subjected to a greater degree of melt extraction prior to emplacement.

Furthermore, gabbro and basalt from the SAO have N-MORB- or arc-like geochemical characteristics that reflect the incorporation of crustal materials into the mantle source, suggesting that this ophiolite formed in a continental marginal back-arc basin setting. In comparison, the less pronounced depletions in trace elements and PGEs, as well as the restricted $^{187}Os/^{188}Os$ isotopic compositions of NJO serpentinized peridotites, suggest that they formed in a fore-arc setting. The contrasting geochemical characteristics of the two ophiolite suites indicate that they were generated during distinct stages of convergence along the southeastern margin of the Yangtze Block. Our results show that ophiolite suites produced within a single orogenic cycle could preserve diverse geochemical characteristics, and may provide insights into the initiation and cessation of continental amalgamation.

1. Introduction

Ophiolites are typically located along suture zones in collision- and accretion-type orogenic belts and represent the remnants of ancient oceanic lithosphere. They can provide crucial constraints on the history of continental convergence (Dewey and Bird, 1971; Dilek and Furnes, 2011; Hébert et al., 2012; Lister and Forster, 2009; Moores et al., 1984; Nicolas, 1989; Santosh et al., 2012, 2013; Taylor and McLennan, 1995). The classical ophiolite succession is commonly dismembered within individual ophiolites as a result of post-emplacement tectonism, leading to possible confusion during the interpretation of original structures (e.g., Morris et al., 2002). More seriously, this issue is further complicated where multistage ophiolite suites or mantle tectonites occur in the same or adjacent areas.

This study focuses on the eastern segment of the Jiangnan Orogen within the South China Block, which contains two Precambrian ophiolite suites, namely the South Anhui ophiolite (SAO) and the Northeast Jiangxi ophiolite (NJO) (Bai et al., 1986; Wang et al., 2007, 2010, 2012; Zhao and Cawood, 1999, 2012; Zhou and Zhu, 1993; Zhou et al., 2004). Previous Sm–Nd studies suggested that the ophiolites

* Corresponding author.
E-mail address: wxl@nju.edu.cn (X.-L. Wang).

https://doi.org/10.1016/j.precamres.2017.12.042
Received 31 August 2016; Received in revised form 24 December 2017; Accepted 28 December 2017
Available online 29 December 2017

formed between the late Mesoproterozoic and early Neoproterozoic (Chen et al., 1991; Li et al., 1997; Zhou and Wang, 1988; Zhou and Zhao, 1991; Zhou et al., 1989). However, more recent *in situ* zircon U–Pb dating results indicate that the SAO formed at ca. 830 Ma (Ding et al., 2008; Zhang et al., 2012, 2013). This age is a bit younger than expected, as it is consistent within errors with the timing of deposition of the surrounding sedimentary sequences (860–820 Ma; Wang et al., 2014; Xue et al., 2010) and the crystallization ages of the strongly peraluminous granitoids (ca. 830–820 Ma; Wang et al., 2014) that are in tectonic contact with the SAO. Previous studies have also suggested that the SAO and NJO complexes share the characteristics of supra-subduction zone (SSZ) type ophiolites and formed in different tectonic settings (Ding et al., 2008; Li et al., 1997, 2003; Wang et al., 2004, 2007, 2012, 2013, 2014; Wu, 2007; Zhang et al., 2012, 2013). However, the specific tectonic environment in which they formed remains uncertain. In particular, the new SAO age data require a thorough re-evaluation of the tectonic settings of the two ophiolites, and any proposed model must reconcile the available field, geochemical, and geochronological data from the ophiolites and associated rocks. As such, more research on these ophiolite suites is required to constrain their formation history and tectonic significance.

Here we present detailed field and petrographic observations coupled with mineral compositions and whole-rock geochemical, Re–Os isotopic, and platinum group element (PGE) geochemical data from the SAO and NJO. In addition, we report SHRIMP zircon U–Pb ages from SAO samples. These data indicate that the two ophiolite suites are geochemically distinct. We confirm that the SAO and NJO formed in back-arc and fore-arc settings, respectively, during Neoproterozoic amalgamation along the southeastern margin of the Yangtze Block.

2. Geological background and sampling

The South China Block (SCB) is separated from the North China Craton to the north by the Qinling–Dabie Orogen and from Tibet to the west by the Songpan–Ganze and Panxi belts (Wang et al., 2012). The SCB preserves evidence for multiple orogenic and crustal reworking events since the Neoproterozoic, recording the construction of East Asia. It was originally formed through amalgamation of the Yangtze and Cathaysia blocks along the ENE-trending Jiangnan Orogen (Fig. 1a; Charvet et al., 1996; Wang et al., 2007, 2012; Zhang and Zheng, 2013; Zhao and Cawood, 1999, 2012; Zheng et al., 2008; Zhou and Zhu, 1993; Zhou et al., 2004). Previous studies indicated that this amalgamation was recorded by a suite of arc volcanics and two ophiolite suites (SAO and NJO) in the eastern Jiangnan Orogen, and continental arc rocks and highly peraluminous post-collisional granitoids that occur throughout the orogen (Wang et al., 2014; Zhang and Zheng, 2013).

The SAO crops out in a ca. 40-km-long NNE-trending zone within the eastern Jiangnan Orogen (Fig. 1b). It was tectonically emplaced into the flysch-like sedimentary sequence of the Shangxi Group (Fig. 1d). Outcrops of the SAO have been reported in the villages of Shexian, Liangyuan, Fuchuan, Futangkeng, Tangchuan, and Fangcun, and are particularly well exposed in the Fuchuan and Futangkeng areas (Fig. 1d; Zhou et al., 1989). The SAO comprises, from bottom to top, a layer of tectonized mantle peridotite, cumulate units, a volcanic sequence, and minor chert (Fig. 1d). The peridotite is dominated by harzburgite with minor dunite, pyroxene-bearing dunite, and pyroxenites. The mafic layer is dominated by gabbro (Figs. 2c–d and 3a–d) and the volcanic sequence comprises pillow basalts with minor spilite and keratophyre units (Zhou, 2013).

A total of 33 samples were obtained along two profiles in the Fuchuan and Futangkeng areas, including 18 serpentinized peridotites, 6 basalts, and 9 gabbro pegmatites. Rocks in these areas have undergone significant serpentinization and lack clear relationships between the gabbro pegmatites (here after referred to as gabbros) and peridotites (Fig. 2d). Rare mafic dykes and lenses/veins of leucogranite crop out within the SAO serpentinized harzburgite.

Thin section observations indicate that almost all primary olivine and pyroxene grains in SAO samples have been replaced by serpentine and chlorite. Chrome-spinel is observed in some samples, typically displaying xenomorphic textures (Fig. 3e), indicative of late alteration. A few samples contain isolated relict olivine (100–1600 μm; Fig. 3f) and orthopyroxene fragments (600–2500 μm; Fig. 3f). Some relict orthopyroxene grains enclose olivine, suggesting their formation at the expense of the latter (Fig. 3f).

The NJO suite stretches about 100 km also in a NNE direction, with the main outcrops in the Zhangshudun, Xiwan, Maoqiao, and Zhongcun areas (Fig. 1c). We focused on the first two of these areas and collected 18 samples of serpentinized peridotite. Gabbro and basalt units are rare within this ophiolite. Although we did not obtain any mafic samples, Zhang et al. (2015) analyzed gabbro blocks and diabase dykes from the NJO. The NJO suite was tectonically emplaced within lower-greenschist-facies slates and phyllites of the Zhangcun Group, which correlate with the ca. 860–830 Ma Shuangqiaoshan Group in northeast Jiangxi Province and the Shangxi Group in south Anhui Province (Chen et al., 1991; Gao et al., 2009; Li et al., 1997, 2008; Wang et al., 2014; Xu and Zhou, 1992). The NJO suite is highly dismembered and comprises serpentinized peridotite along with rare cumulate gabbro, dolerite, diorite, plagiogranite, spilitic keratophyre, basalt, and chert (Fig. 2a–b; Li et al., 1997; Zhou and Zhao, 1991). Shu et al. (1993) identified a small block of blueschist ($> 10\ m^2$) in the Xiwan area that enabled the identification of a high-pressure metamorphic event (~ 12 Kbar, 300 °C–400 °C; Shu et al., 1993; Zhou et al., 1989). Thermal metamorphism also occurred within the NJO, as evidenced by the occurrences of garnet, tremolite, and diopside hornfels (Zhou et al., 1989). A few samples from the Xiwan outcrop preserve relict isolated primary olivine and pyroxene grains (Fig. 3g–h). Similar to the SAO samples, some olivine grains are surrounded by orthopyroxene, suggesting that orthopyroxene formed at the expense of olivine (Fig. 3h).

3. Analytical procedures

3.1. Electron microprobe analyses of mineral compositions

Electron microprobe analyses (EMPA) of mineral compositions of the olivine, orthopyroxene (from the SAO and NJO) and chrome spinel (from the SAO) were carried out with the JXA-8100 (JEOL) at the State Key Laboratory for Mineral Deposits Research (MiDeR), Nanjing University (NJU). The conditions of analyses were at a 15 kV accelerating voltage and a 2×10^{-8}A beam current. The peak and background counting times for most elements were 10 s and 5 s, except for Mn (peaks were 20 s, backgrounds were 10 s). All data were corrected with standard ZAF correction procedures. The analytical precision is generally better than 2% for all elements. The results of two types of pyroxene and chrome spinel are listed in Table S1 and Table S2 respectively in the Supplementary Appendix A, and the mineral formulae were calculated using a Pasform program (Bjerg et al., 1995).

3.2. Whole-rock major and trace element analyses

Whole-rock major element analyses of most samples were obtained using an ARL9800XP + X-ray fluorescence spectrometer (XRF) at the MiDeR, NJU. The glass discs were prepared by fusion of a mixture with an alkali flux consisting of a mixture of lithium tetraborate, lithium metaborate and lithium bromide at 1050 °C. Analyses were carried out with an accelerating voltage of 50 kV and a beam current of 50 mA. Standards (GSR-3) were prepared using the same procedure to monitor the analytical precision. The analytical precision is generally better than 2% for all elements.

Whole-rock trace elements were analyzed using a Perkin-Elmer ELAN DRC-e ICP-MS at the State Key Laboratory of Ore Deposit Geochemistry, Institute of Geochemistry, Chinese Academy of Sciences, Guiyang. The powdered samples (50 mg for each sample) were

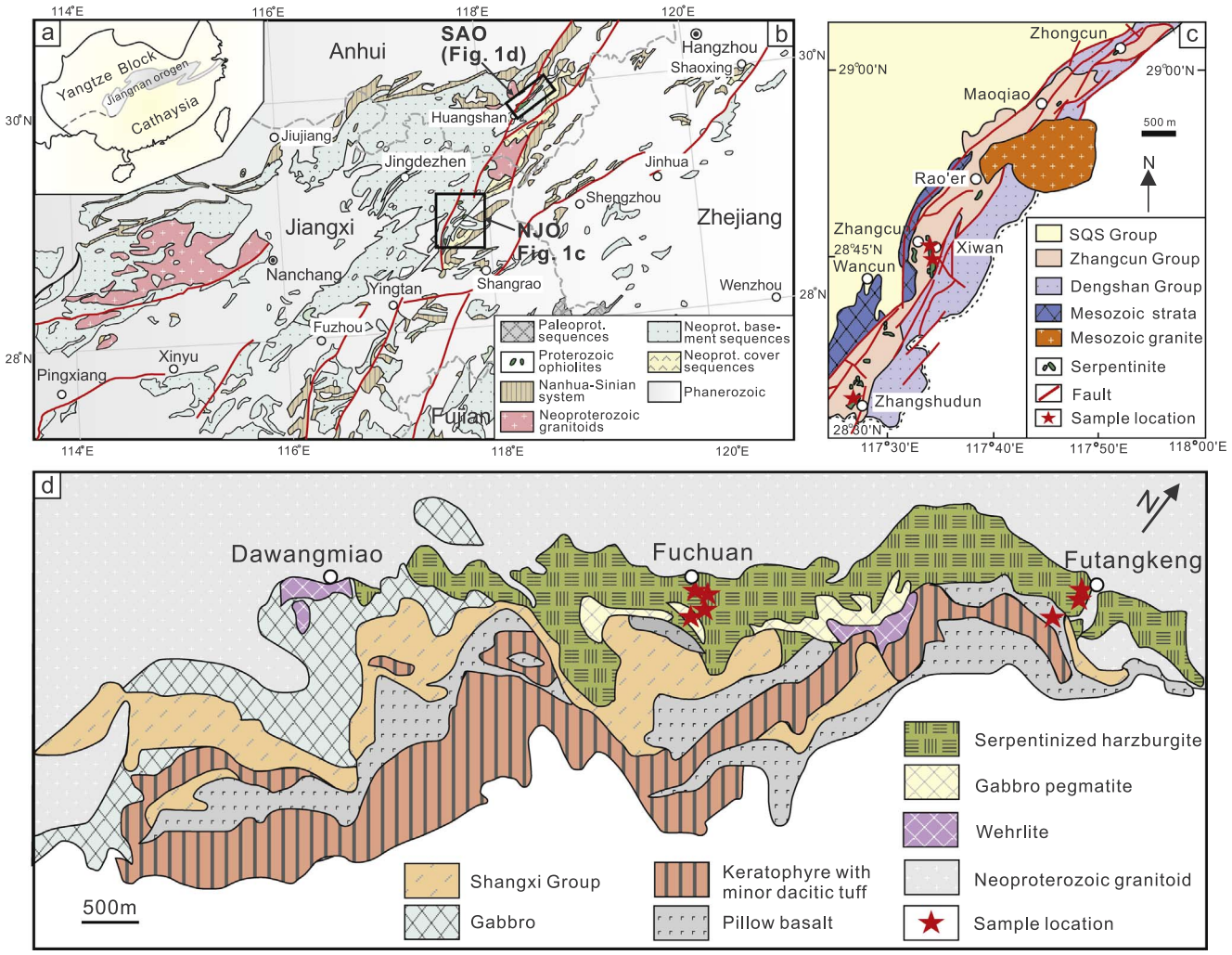

Fig. 1. Simplified geological map showing the distributions of the South Anhui ophiolite (SAO) and the Northeast Jiangxi ophiolite (NJO). (a) Sketch map of South China and the Jiangnan Orogen. (b) Geological map of the eastern segment of the Jiangnan orogen (modified after Wang et al., 2012). (c) Geological map of the NJO (modified after Wang et al., 2016). (d) Geological map of the SAO (modified after Ding et al., 2008). Sampling locations are indicated by red stars. (For interpretation of the references to colour in this figure legend, the reader is referred to the web version of this article.)

dissolved in high-pressure Teflon bombs using HF + HNO_3 mixture for 48 h at ~190 °C (Qi et al., 2000). Rh was used as an internal standard to monitor signal drift during counting. The international standards GBPG-1, OU-6, and the Chinese National standards GSR-1 and GSR-3 were used for monitoring analytical quality. The analytical precision is generally better than 5% for trace elements.

Whole-rock major and trace element analyses for the samples from the SAO and NJO are listed in Table S3 in the Supplementary Appendix A.

3.3. SHRIMP zircon U–Pb dating

Zircons were separated from the crushed rock of 10SX-3-1 using conventional heavy liquid and magnetic techniques. Random zircon grains were mounted in epoxy resin, and polished to expose their cores for analysis. Zircon U–Pb isotopic compositions were conducted using the SHRIMP II ion microprobe at the Beijing SHRIMP Center under standard operating conditions (5-scan cycle, 2nA primary O^{2-} beam, mass resolution of 5000). U–Th–Pb isotopic ratios were calibrated relative to standard zircon TEMORA-2 with $^{206}Pb/^{238}U = 0.0668$ corresponding to 417 Ma (Black et al., 2003), and the absolute abundances were calibrated to the standard zircon SL13. Analyses of the TEMORA standard zircon were interspersed with those of unknowns, following operating and data processing procedures similar to those described by Williams (1998). Measured compositions were corrected for common Pb using the ^{204}Pb-method. Uncertainties on individual analyses are reported at 1σ level, and mean ages for pooled $^{206}Pb/^{238}U$ results are quoted at 95% confidence level. The SHRIMP zircon U-Th-Pb isotopic data are given in Table S4 in the Supplementary Appendix A.

3.4. PGE and Re-Os analyses

PGE concentrations and Re-Os isotopes were determined by a Bruker Aurora M90 inductively-coupled plasma mass spectrometry (ICP-MS) following the method of Qi et al. (2007, 2013). The sensitivity for the instrument was adjusted to 350,000 cps for 1 ng/mL ^{115}In and 150,000 cps for 1 ng/mL of ^{232}Th.

Five grams of sample and appropriate amounts of the enriched isotope spike solution containing ^{185}Re, ^{190}Os, ^{101}Ru, ^{193}Ir, ^{105}Pd and ^{194}Pt were carefully weighed and placed in a cooled (with an ice water bath) re-usable Carius tube (Qi et al., 2013). 5 mL of HCl and 15 mL of cooled HNO_3 were added. The sealed re-usable Carius tube was placed in a stainless steel jacket heated to 240 °C for about 24 h. After slowly cooling down in air to room temperature, the Carius tube was further cooled in a refrigerator for 2 h and then opened for in-situ Os distillation. The Os trapped solution was used for ICP-MS measurement using Ir for mass fractionation correction.

After distillation, the residual solution was transferred to a 125 mL

Fig. 2. Field photographs of the two ophiolite suites. (a) Serpentinites of the NJO at the Zhangshudun outcrop with rounded rodingite blocks. (b) Serpentinites of the NJO at the Xiwan outcrop with rounded blocks showing harzburgites containing relict primary olivine and orthopyroxene grains. (c) Pillow basalts of the SAO at the Futangkeng outcrop. (d) Gabbro pegmatite in contact with serpentinized harzburgite at the Fuchuan outcrop.

Savillex Teflon beaker and evaporated to dryness twice with 5 mL of concentrated HCl to remove HNO_3. The resultant solution was then dissolved with 40 mL of 2 mol 1:1 HCl and transferred to a 50 mL tube for centrifuging. About 10 mL of the centrifuged solution was used to separate Re from the matrix using AG 1-X8 anion exchange resin and measured Re by ICP-MS.

The remaining 30 mL aliquot of this solution was used to pre-concentrate PGEs by Tecoprecipitation. A mixed ion exchange column which contains a Dowex 50 WX 8 cation exchange resin and a Ln extraction chromatograph resin was used to remove the main interfering elements, including Cu, Ni, Zr and Hf, after the Te-coprecipitation (Qi et al., 2004). The elution solution was used for measuring Pt, Pd, Ru, and Ir by ICP-MS. Whilst ^{194}Pt was used as the internal standard to calculate the concentration of the monoisotope element Rh (Qi et al., 2004). The blank corrected results of reference materials, WGB-1 and UMT-1, are in a good agreement with the certified values and the reported values (Meisel and Moser, 2004). Whole-rock Re-Os isotopic and PGE data of the SAO and NJO complexes are shown in Table S5 in the Supplementary Appendix A.

3.5. Zircon O isotope analyses

Oxygen isotope ratios were analyzed in the dated portions of the same zircons with the SHRIMP II of the Beijing SHRIMP Center of China Academy of Geological Sciences. Each $^{18}O/^{16}O$ analysis took approximately 7 min, including about 5 min for ion beam tuning and the measurement of electrometer baselines and 2 min for oxygen isotope measurement. The analytical procedures and conditions are similar to those described by Wan et al. (2013). The Cs^+ primary ion beam was accelerated with an intensity of ca. 3 nA. The spot diameters were 20 μm. The TEMORA-2 zircon ($\delta^{18}O$ = 8.20%; Black et al., 2004) was used for calibration of instrumental mass fractionation (IMF) as the reference material. The zircon O isotopic results are listed in Table S6 in the Supplementary Appendix A.

4. Results

4.1. Mineral geochemistry

Accessory chrome-spinel, ferritchromite, and magnetite are observed within serpentinized harzburgite samples from the SAO. However, most chrome-spinel grains have been altered to ferritchromite. Backscattered electron and microscope observations indicate that chrome-spinel is xenomorphic (Fig. 3e). In addition, EMPA analyses show that SAO chrome-spinel contains high Cr_2O_3 (44.3–46.9 wt%), moderate Al_2O_3 (22.9–24.9 wt%), and low TiO_2 (0.004–0.045 wt%) concentrations. They have Cr# [$= 100 \times (Cr^{3+}/(Cr^{3+} + Al^{3+}))$] values of 54.8–57.5, consistent with the chrome-spinel within samples FC-4B and FC-9A reported by Ding et al. (2008), but lower than another sample reported in the same study (FC-22, mean = 66.6; Ding et al., 2008). However, lower Cr# values may be related to late alteration, suggesting that spinel from sample FC-22 has the composition most closely resembling that of the primary spinel.

Relict olivine fragments within the SAO complex contain high MgO (47.0–51.8 wt%), variable Al_2O_3 (0.004–4.28 wt%), and low CaO (0.034–2.29 wt%) concentrations, and yield high Mg# [$100 \times Mg/(Mg + Fe^{2+})$] values (91.4–92.1; Table S1). Relict orthopyroxene grains in the SAO harzburgites have a restricted range of MgO contents of 31.5 to 35.2 wt%, and slightly higher Mg# values of 91.7–92.5 (mean = 92).

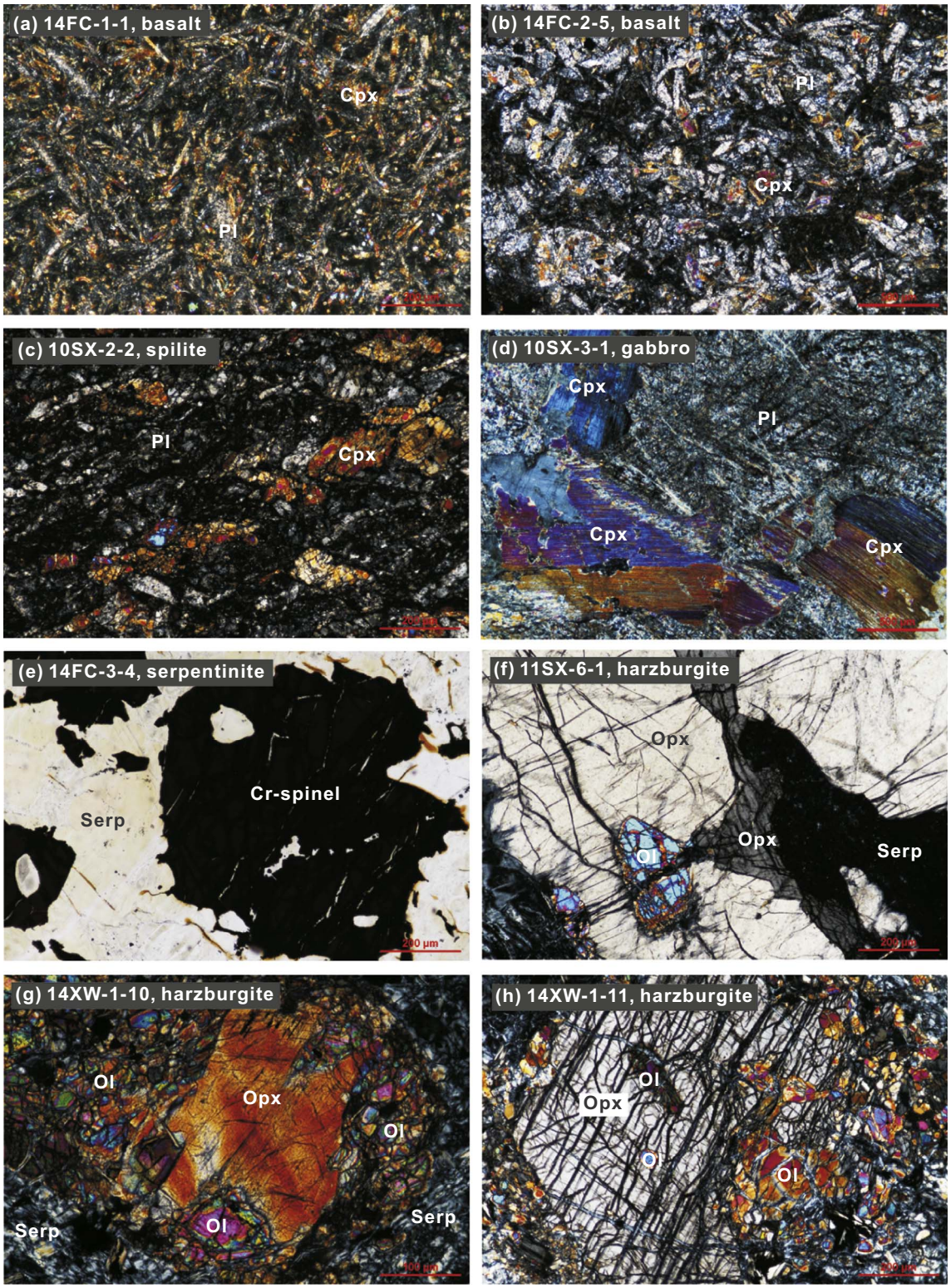

Fig. 3. Photomicrographs of representative samples from the SAO (a–f) and NJO (g–h). Pl = plagioclase; Cpx = clinopyroxene; Opx = orthopyroxene; Serp = serpentine.

In contrast to the SAO, the NJO complex records a greater degree of serpentinization that is evident in both field and microscope observations. No previous studies have reported fresh primary mafic minerals within the NJO serpentinized peridotites. Here, we present the first results of relict orthopyroxene and olivine fragments from the NJO within our samples 13XW-1-1 and 13XW-1-7 (Fig. 5e–f). These orthopyroxene grains contain MgO concentrations (31.1–35.3 wt%) similar to those reported from the SAO, but show variable CaO contents (0.40–2.29 wt%). Their Mg# values (90.0–92.9, mean = 91.0) are slightly lower than those of SAO orthopyroxene. Similarly, relict olivine grains from the NJO complex have lower MgO (47.9–50.9 wt%) contents and Mg# values (88.5–89.9, mean = 89.5) than those from the SAO.

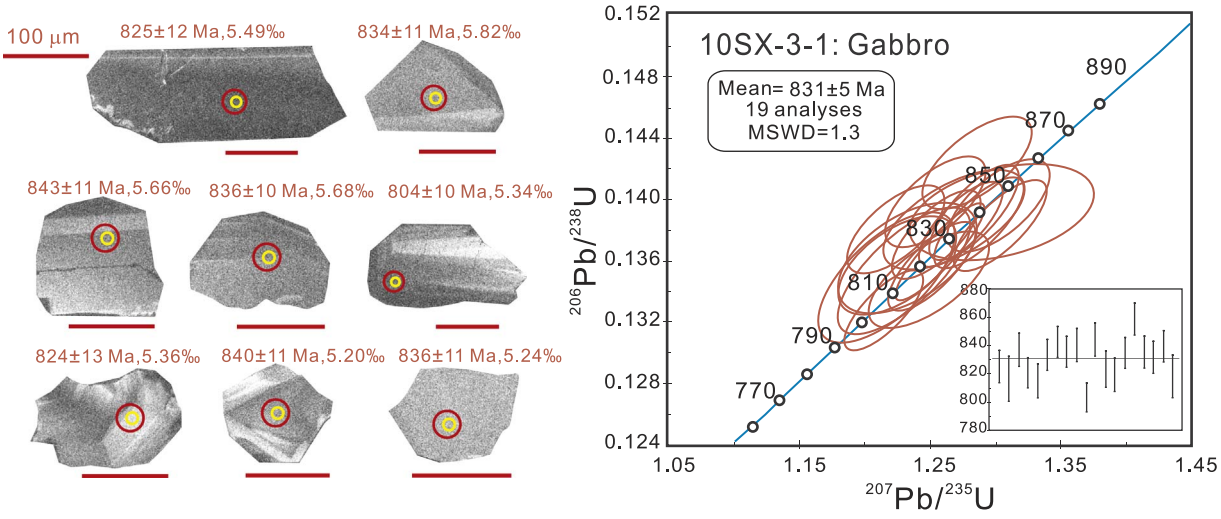

Fig. 4. Representative cathodoluminescence (CL) images and zircon U–Pb concordia plot for a gabbro sample (10SX-3-1) from the SAO. Small yellow circles represent O isotope analysis spots, and large red circles show locations analyzed for U–Pb isotope analyses. (For interpretation of the references to colour in this figure legend, the reader is referred to the web version of this article.)

4.2. SHRIMP zircon U–Pb dating and O isotopes

Separated zircon grains from the gabbro sample 10SX-3-1 are generally euhedral and 100–200 μm long. In cathodoluminescence (CL) images, they are bright and show broad to weak oscillatory zoning, suggesting a magmatic origin (Fig. 4). Nineteen spot analyses on zircons from this sample yielded a weighted mean $^{206}Pb/^{238}U$ age of 831 ± 5 Ma (n = 19; MSWD = 1.3; Fig. 4), consistent with previously reported ages for the complex (842 ± 12 Ma, Ding et al., 2008; 833 ± 7 Ma, Yin et al., 2013; 824 ± 3 Ma, Zhang et al., 2012; 819 ± 3 Ma to 827 ± 3 Ma, Zhang et al., 2013). The analyzed zircons have $\delta^{18}O$ values ranging from 4.75‰ to 6.77‰ (Fig. 5; Table S6) and yield a weighted mean value of 5.49 ± 0.22‰ (n = 19, MSWD = 2.6; Fig. 5), consistent with typical mantle zircon compositions (5.3 ± 0.6‰; Valley et al., 1998).

The age ca. 830 Ma reported here is absolutely younger than the previously suggested late Mesoproterozoic to early Neoproterozoic Sm–Nd isochron age for the complex. It is also younger than the new zircon U–Pb ages (ca. 968 ± 23 Ma and 970 ± 21 Ma for the plagiogranites and 1009 ± 5 Ma to 993 ± 12 Ma for the gabbro dykes; Gao et al., 2009; Li et al., 1994, 2017; Wang et al., 2015) of the NJO complex.

4.3. Whole-rock geochemistry

4.3.1. Major elements

Eighteen serpentinized peridotite samples from the SAO complex yield SiO_2 and MgO contents of 35.8–37.8 wt% and 36.6–42.1 wt%, respectively, and Mg# values of 87.6–91.7 (Table S3). In contrast, 18 serpentinized peridotite samples from the NJO complex contain slightly high concentrations of SiO_2 (38.7–43.6 wt%) and relatively uniform MgO contents (34.3–38.5 wt%) and Mg# values (88.4–91.5). Basalt samples from the SAO complex contain low concentrations of TiO_2 (0.56–0.86 wt%) and can be divided into two groups according to their Al_2O_3contents. Low-Al basalts yield homogenous Al_2O_3 (15.3 wt%) and SiO_2 (48.7–50.1 wt%) contents, whereas high-Al basalts contain 16.3–18.0 wt% Al_2O_3 and 49.4–55.3 wt% SiO_2. SAO gabbros contain 44.1–48.3 wt% SiO_2 and yield variable CaO (14.6–20.9 wt%), Al_2O_3 (9.58–18.4 wt%), and MgO (8.7–16.4 wt%) contents, indicating variable proportions of plagioclase and olivine in the CIPW normative (norm) mineralogy.

Although peridotites from both ophiolites are highly altered, their CIPW normative mineralogy and relict primary mineral assemblages still offer insights into their protolith compositions, indicating these samples were originally harzburgite and minor dunite (Fig. 6).

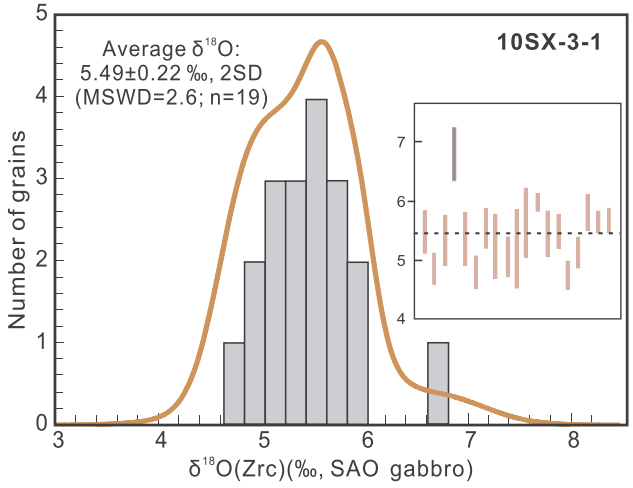

Fig. 5. SIMS zircon O isotopic compositions for the gabbro sample 10SX-3-1.

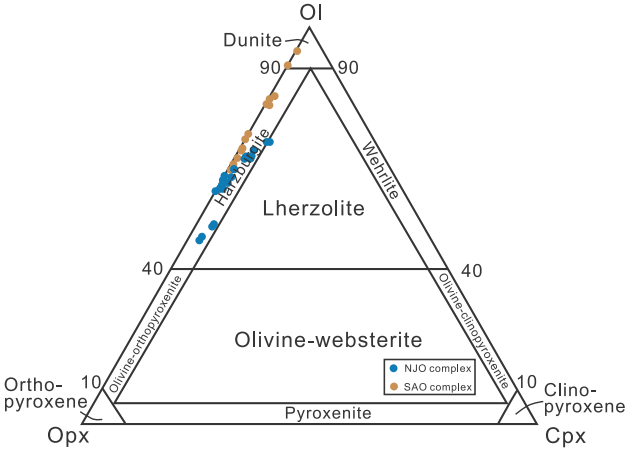

Fig. 6. Ol–Cpx–Opx plot for serpentinized peridotites from the SAO and NJO complexes.

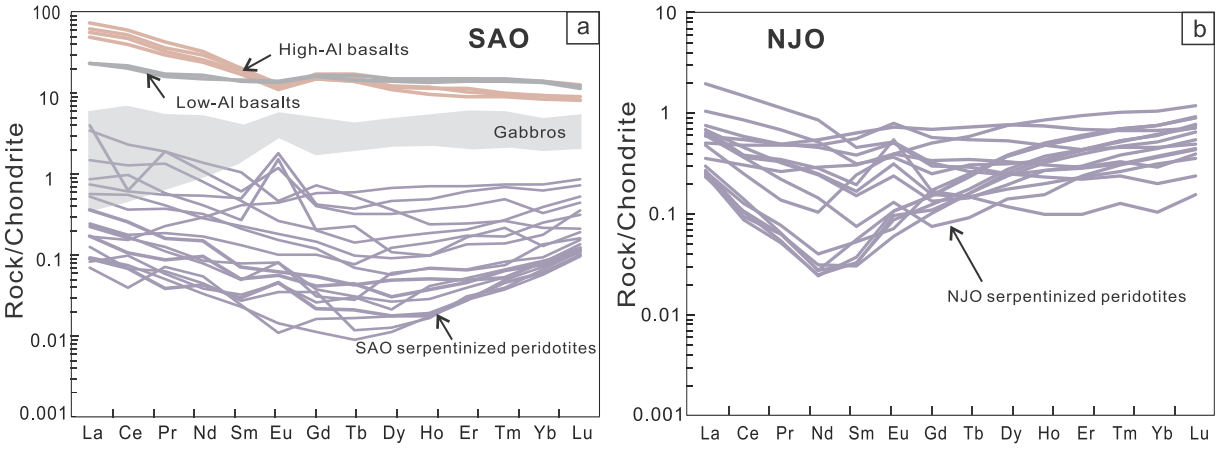

Fig. 7. Chondrite-normalized REE patterns for samples from the SAO and NJO. (a) Basalt, gabbro, and serpentinized peridotite from the SAO complex. (b) Serpentinized peridotite from the NJO complex. Chondrite data are from Sun and McDonough (1989).

4.3.2. Trace elements

In contrast to the major element data presented above, we observe considerable variations in trace element concentrations among rocks from the SAO and NJO (Table S3). SAO serpentinized peridotites contain highly variable concentrations of Cr (956–3076 ppm) and Ni (1670–2378 ppm), in contrast to the relatively uniform concentrations of these elements in NJO serpentinized peridotites (Cr = 1030–2730 ppm and Ni 1560–1990 ppm). In contrast to the peridotites, the SAO gabbros contain low but variable concentrations of Cr (89–936 ppm) and Ni (99–1760 ppm).

Peridotites from both the SAO and NJO yield U-shaped rare earth element (REE) patterns, although SAO peridotites are depleted in middle REE (MREE; Sm–Ho), whereas the NJO samples are depleted in Pr–Eu and enriched in Dy–Lu (Fig. 7a–b). The SAO high-Al basalts are highly enriched in light REE (LREE) and the low-Al basalts have REE and trace element compositions similar to those of typical island arc basalts (IAB) (Figs. 7a and 8). In contrast, SAO gabbros are compositionally similar to normal mid-ocean ridge basalts (N-MORB), recording slight depletions in LREE and flat middle and heavy REE (HREE) patterns (Fig. 7a). The gabbro samples also show weakly positive Eu anomalies that are indicative of plagioclase accumulation. In addition, these gabbros show positive Sr, U, and K, and variable Rb and Ba anomalies (Fig. 8), which indicate crustal assimilation.

4.3.3. Os isotopes

Whole-rock Os isotopic compositions were determined for 13 representative samples from the SAO complex and 7 representative serpentinized peridotites from the NJO complex (Table S5).

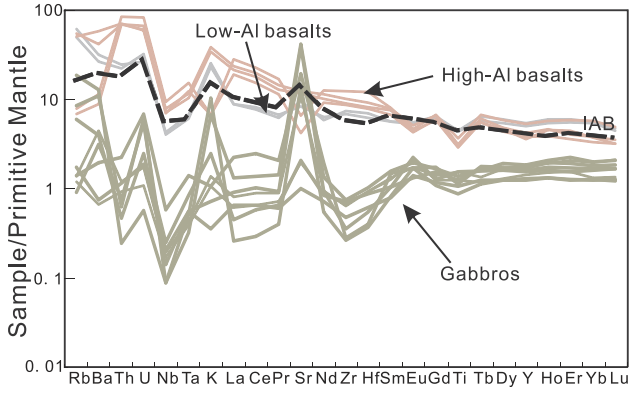

Fig. 8. Primitive-mantle-normalized trace element compositions for SAO basalts and gabbros. Primitive mantle data are from McDonough and Sun (1995). The dotted line shows the composition of typical island arc basalts (IAB) (Kelemen et al., 2003).

All samples have low Re concentrations (SAO = 0.02–0.17 ppb; NJO = 0.07–0.84 ppb). The SAO serpentinized peridotites contain variable concentrations of Os (0.04–4.04 ppb) that are generally lower than those of NJO samples (2.19–4.12 ppb). These serpentinized peridotites have chondrite-like ($^{187}Os/^{188}Os$ = 0.1281; Walker et al., 2002) $^{187}Os/^{188}Os$ ratios of 0.116–0.144 and 0.120–0.132 for the SAO and NJO complexes, respectively. However, SAO and NJO samples yield calculated mean $^{187}Re/^{188}Os$ ratios of 0.69 and 0.52, respectively, slightly higher than the chondritic value (0.421; Walker et al., 2002).

Seven gabbro samples from the SAO complex have low Os concentrations (0.01–0.22 ppb) and higher $^{187}Os/^{188}Os$ ratios than the peridotites (0.13–0.28). The gabbro samples contain high Re concentrations and yield elevated $^{187}Re/^{188}Os$ ratios (0.06–82.8).

4.3.4. PGE geochemistry

Serpentinized peridotites from both complexes have highly variable PGE contents, with total PGE concentrations of 2–16 and 7–31 ppb, respectively. In contrast, except one gabbro sample with high Pd contents, the SAO gabbro samples generally have PGEs lower than peridotite samples and contain positively sloping Ir–Pd distribution patterns (Fig. 9a) with elevated Pd/Ir ratios (up to 964). Compared with the Mamonia spinel lherzolites of Cyprus and Mesozoic ophiolites from Troodos, Cyprus (Batanova et al., 2008; Garuti et al., 1997), the SAO peridotites contain lower concentrations of PGE (less than primitive mantle; Fig. 9a). In comparison, the PGE contents of NJO samples are similar to those of Troodos ophiolites (Fig. 9b). The SAO peridotites are depleted in Pt–Pd, with an average Pt concentration (1.19 ppb) that is significantly lower than that of the NJO samples (7.69 ppb).

5. Discussion

5.1. PGEs constraints on mantle characteristics

As the SAO and NJO might form during distinct tectonic episodes, they likely preserve the compositions of two different mantle regions. Previous research has focused on the geochronology and geochemistry of basaltic rocks from the two ophiolite suites (Chen et al., 1991; Ding et al., 2008; Li et al., 1997; Zhang et al., 2012, 2013; Zhou and Wang, 1988; Zhou and Zhao, 1991). However, their petrogenesis and tectonic affinities are poorly constrained, and no studies have compared the PGE composition of the two suites.

Prior to any in-depth interpretation, it is necessary to discuss the influence of low-temperature alteration processes on whole-rock PGE concentrations in our samples. Ultramafic rocks that have undergone oxidative weathering are generally regarded as unsuitable for whole-rock geochemical analysis that aims to constrain high-temperature

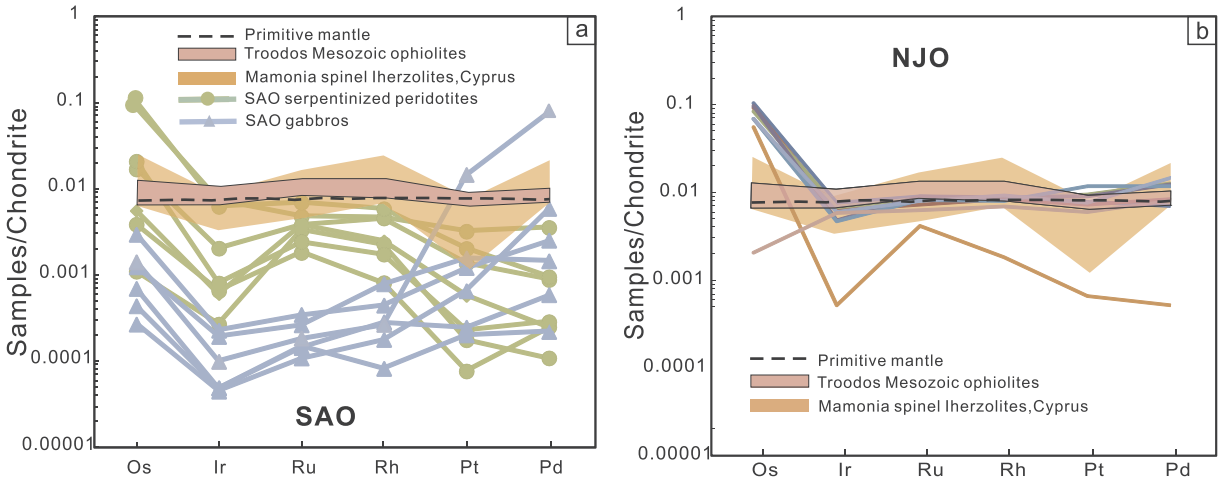

Fig. 9. Chondrite-normalized PGE concentrations for samples from the SAO (a) and NJO (b). The dotted line indicates the composition of the primitive mantle (McDonough and Sun, 1995). The light gray field indicates the compositions of the Mamonia spinel lherzolites (Batanova et al., 2008) and the dark gray field indicates the compositions of Mesozoic ophiolites from Vourinos, Ligura, and Troodos (Garuti et al., 1997).

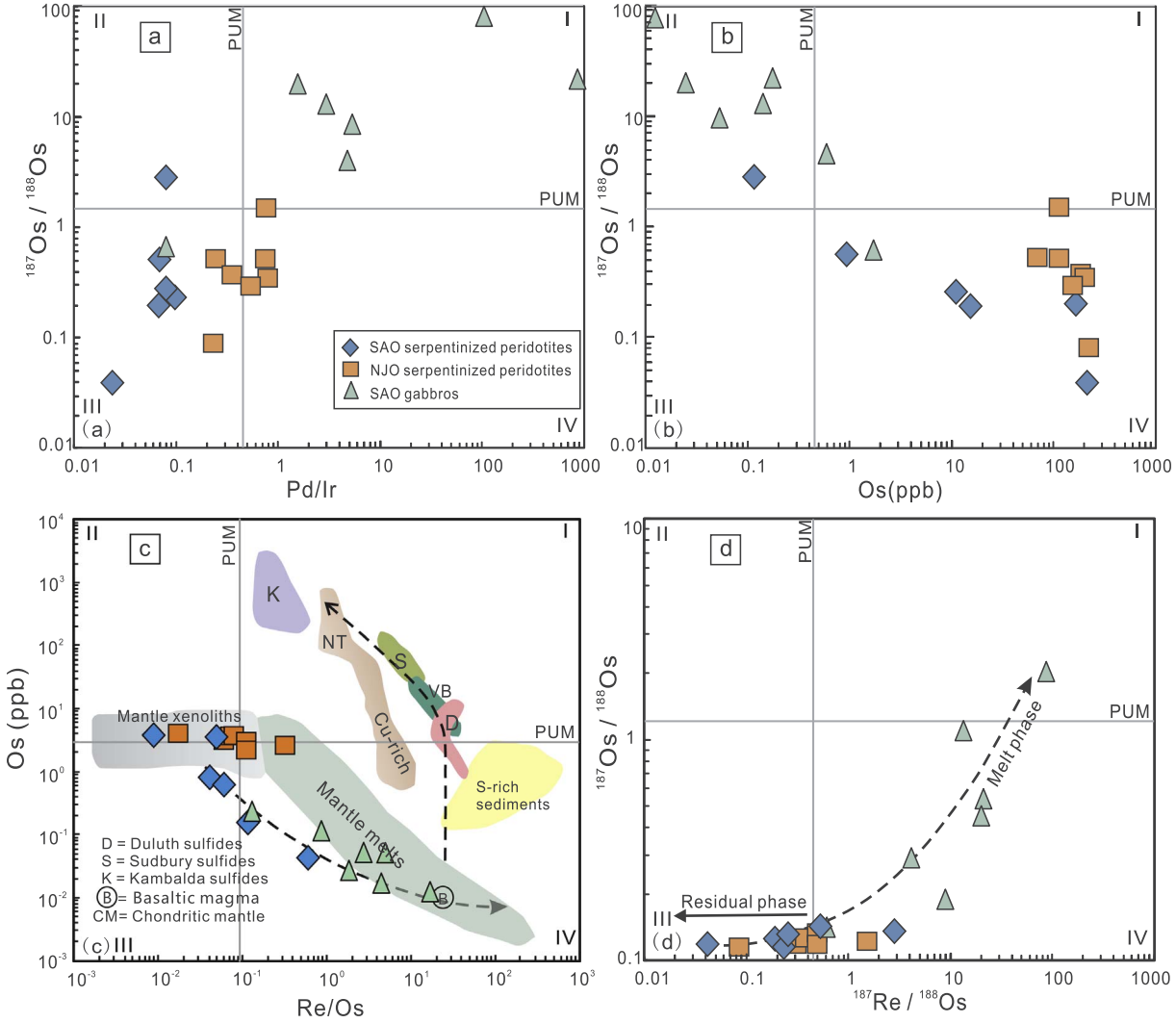

Fig. 10. Re–Os isotopic variations for samples from the SAO and NJO suites. (a) $^{187}Os/^{188}Os$–Pd/Ir diagram. (b) $^{187}Os/^{188}Os$–Os diagram. (c) Re/Os–Os diagram (modified after Lambert et al., 1998). (d) $^{187}Re/^{188}Os$–$^{187}Os/^{188}Os$ diagram.

processes, as sulfides within such samples are likely to have been partially or totally oxidized (Becker and Dale, 2016). However, such processes are unlikely to have affected the PGE concentrations of the investigated samples, as they lack the coloration that typically indicates secondary ferric weathering. Furthermore, the analyzed samples contain few iron oxide grains. Serpentinization reactions are thought to

have little influence on PGE concentrations, as they typically occur under reduced conditions (Brandon et al., 2000; Büchl et al., 2002; Rehkämper et al., 1999; Snow and Reisberg, 1995; Snow and Schmidt, 1998). Moreover, PGE concentrations within the investigated peridotites are not correlated with loss on ignition (LOI) values, indicating little influence of serpentinization on their PGE concentrations. PGE concentrations and ratios are instead correlated with $^{187}Os/^{188}Os$ and Re/Os ratios (Fig. 10a, b).

Samples from the SAO and NJO complexes display distinct chondrite-normalized PGE distribution patterns. The SAO samples have variably negative Ir anomalies and clear Pt–Pd depletions (Fig. 9a), whereas the NJO samples lack evidence for PGE fractionation (Fig. 9b). PGEs can be classified, based on melting behavior and temperature, into the Pd-subgroup (PPGE; including Pt, Pd and Rh) and the Ir-subgroup (IPGE; including Os, Ir and Ru). Firstly, the influence of sulfides needs to be considered when interpreting PGE differentiation. Available studies have shown that partial melting has a variable effect on the extraction of PGE from different sulfide minerals. Based on these data, sulfides can be divided into two types based on their occurrence and composition (Alard et al., 2000, 2002). Type-1 sulfides represent rounded Fe–Ni-enriched minerals that contain high concentrations of IPGE and low concentrations of PPGE, and are commonly observed as inclusions within other minerals. In comparison, type-2 sulfides represent Cu–Ni-enriched interstitial phases associated with late-formed clinopyroxene and spinel, and typically contain low concentrations of IPGE and high concentrations of PPGE (Alard et al., 2000, 2002; Ballhaus et al., 2006; Bockrath et al., 2004; Luguet et al., 2003). During partial melting of mantle peridotite, type-2 sulfides preferentially enter the melt, whereas type-1 sulfides typically remain in the residual peridotites (Alard et al., 2000; Ballhaus et al., 2006; Bockrath et al., 2004; Luguet et al., 2003). Therefore, residual phases in the mantle are commonly enriched in IPGE relative to PPGE. This is consistent with the depletions of IPGE relative to PPGE recorded by the SAO gabbros (Fig. 9a) that were generated during partial melting of peridotites. Especially, one gabbro sample shows a particularly significant fractionation of Pt and Pd (Fig. 9a). In contrast, the SAO peridotites are depleted in PPGE relative to most IPGE (Fig. 9a). The SAO peridotites are also variably depleted in Ir (Fig. 9a), suggesting that most of the sulfides were consumed during early melting processes. Secondly, during partial melting, PPGEs preferentially enter the melt phase whereas the IPGE are retained in residual phases (Barnes et al., 1985; Mitchell and Keays, 1981). Therefore, PPGE and IPGE are differentiated during partial melting. For example, low-degree partial melting will result in a significant depletion of PPGE relative to IPGE within residual mantle phases, yielding a negative sloping chondrite-normalized PGE distribution pattern. Thus, Pt and Pd depletions in the SAO samples likely resulted from melt extraction.

Generally, all of the serpentinized peridotite samples from the SAO and NJO are enriched in Os relative to the other PGEs (Fig. 9). This is likely to have resulted from the preferential retainment of Os in residual phases during melting, since Os is the most incompatible PGE. Cumulate gabbros in the SAO are also enriched in Os, despite their relatively low PGE concentrations (Fig. 9a). This observation indicates that early-crystallized phases in mantle-derived basaltic melts within ophiolite suites may preferentially incorporate Os. In contrast to the SAO samples, most of the NJO serpentinized peridotites yield flat unfractionated PGE patterns, and no correlation is observed among MgO and Ir, Ru, Pt, or Pd (Fig. 11), suggesting insignificant melt extraction and fluid metasomatism. One NJO sample (13XW-4-3) is depleted in Ir, Pt, and Pd in a similar way to the SAO samples. This suggests that at least some NJO peridotites also underwent low degree of partial melting.

Most of the NJO samples plot close together in the Pd–Ir diagram (Fig. 12a), and they are distinguishable from SAO peridotites in the Pd/Ir–Re/Os diagram (Fig. 12b). The SAO samples have low Pd/Ir ratios and plot within the field of sulfide inclusions in peridotites (i.e., type-1 sulfide inclusions as mentioned above), whereas the NJO peridotites plot in the bulk-rock peridotite field (Fig. 12b). This supports a greater melt extraction in the SAO peridotites than in the NJO.

Despite the significant differences in melt extraction and degree of fluid metasomatism, both SAO and NJO samples underwent melt metasomatism, as revealed by their U–shaped REE patterns and the observation of olivine grains enclosed in orthopyroxene (Fig. 3g–h). Melt metasomatism may also influence PGE concentrations, and some SAO samples yield a positive correlation in a Pd–Ir diagram that trends toward melt compositions (Fig. 12a). In comparison, SAO gabbros define a trend deviating from the SAO peridotites, but which is similar to gabbros and cumulates from the Oman ophiolite. This indicates that the metasomatic agent that interacted with the SAO peridotites was distinct from the melt that produced the SAO gabbros. In addition, only one NJO peridotite sample lies within the trend defined by SAO peridotites, indicating that at least part of the NJO was also subjected to melt metasomatism.

If SAO peridotites underwent significant fluid metasomatism, it is necessary to evaluate its influence on PGE geochemistry and Re–Os isotopes. However, later melt metasomatism makes it difficult to constrain such processes. As the NJO samples that may have undergone a lower degree of fluid metasomatism still preserve concentrated chondrite-like PGE patterns and Os isotopic compositions, we suggest that the influence of fluid metasomatism was insignificant.

5.2. Os isotopic constraints on mantle melting behavior

The Os isotopic data obtained in this study can provide insights into the formation of mantle peridotites in the SAO and NJO areas. The Earth's primitive upper mantle (PUM) has an Os isotopic composition that is within the range of compositions of chondritic meteorites (Meisel et al., 1996). Although Re and Os are both siderophile elements, Re is incompatible and Os compatible during partial melting. Re is therefore enriched in melt phases (e.g., cumulates and lava) during partial melting of peridotite, whereas Os becomes concentrated in residual phases, leading to variations in the concentrations of Re and Os within mantle peridotites and associated melts. Consequently, $^{187}Os/^{188}Os$ ratios can be used to distinguish between residual and melt phases. In SAO samples, we observe a clear trend from serpentinized peridotites to gabbros, with the latter having lower Os concentrations and elevated Re/Os, $^{187}Os/^{188}Os$, and $^{187}Re/^{188}Os$ ratios (Fig. 10). This indicates that the SAO gabbros represent cumulates from mafic melts generated by partial melting of the peridotites. In contrast, the NJO serpentinized peridotites have a restricted range of Os concentrations and $^{187}Os/^{188}Os$ ratios that define a trend in an Os vs. Re/Os diagram that is distinct from that of the SAO samples (Fig. 10c). This provides further evidence that the NJO peridotites underwent a different melting history to that of the SAO peridotites.

Whole-rock Os isotopic compositions may also be affected by melt-peridotite interaction (i.e., metasomatism). A $^{187}Os/^{188}Os$–Al_2O_3 diagram can be used to constrain the timing of melt depletion and evaluate possible melt metasomatism (Becker and Dale, 2016). The NJO samples lie within MORB- and SSZ-type ophiolite fields in the $^{187}Os/^{188}Os$–Al_2O_3 diagram (Fig. 13). Some samples (especially those from the NJO) define a roughly positive linear correlation (Fig. 13), reflecting the primary magmatic characteristics of these rocks (Gao et al., 2002; Handler et al., 1997; Peslier et al., 2000; Reisberg and Lorand, 1995). Two of the NJO samples and some of the SAO peridotites have elevated $^{187}Os/^{188}Os$ ratios (Fig. 13), indicating either the addition of radiogenic Os or the time-integrated addition of Re. Both processes can result from melt-peridotite metasomatism relating to fluxes from a subducting slab. In subduction zone settings, sub-arc mantle-derived melts that incorporate crustal materials commonly have radiogenic Os isotopic compositions and elevated Re concentrations. Their subsequent interaction with mantle peridotite will alter the Os isotopic composition of the peridotites. Melt-rock reactions during melt percolation result in the decoupling of Al_2O_3 concentrations and

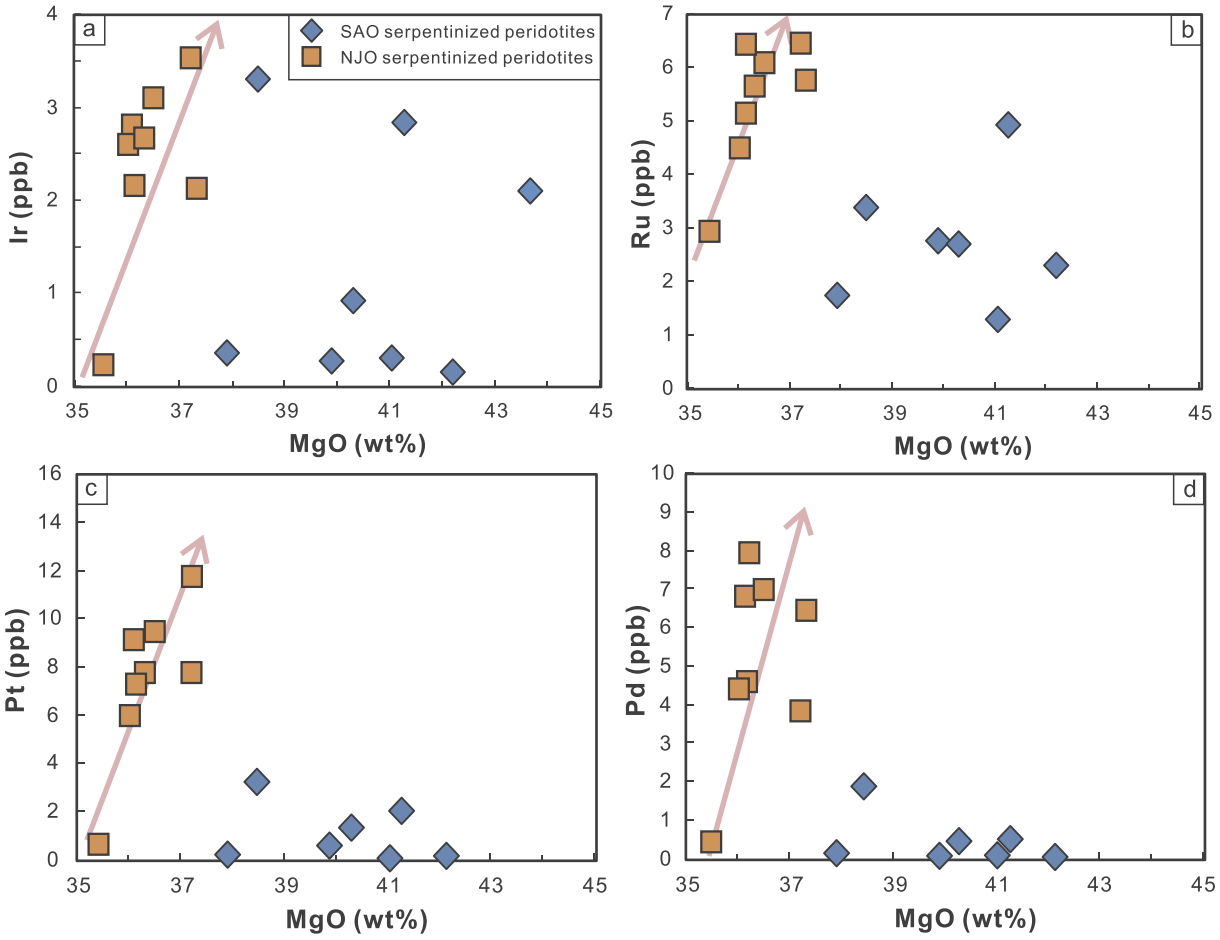

Fig. 11. Variation in PGE with MgO concentrations for the SAO and NJO serpentinized peridotites.

$^{187}Os/^{188}Os$ values, as is the case for SAO peridotites. In addition, the significant amount of melt-related metasomatism recorded in the SAO is consistent with the presence of chromitites in the ophiolite suite, similar to those observed in the Oman Ophiolite. Thus, the SAO may have been influenced by supra-subduction zone melting processes. Such processes were recorded in the Oman Ophiolite by the abundance of podiform chromitite deposits (Boudier et al., 2000; Ishikawa et al., 2002).

5.3. Geochemical constraints on ophiolite subduction zone settings

Most abyssal peridotites and peridotite within convergent margin ophiolites are harzburgite (with minor dunite), whereas lherzolites are more typical of ultra-slow-spreading environments, subcontinental settings, and continent–ocean transitional regions (Becker and Dale, 2016). Therefore, a high degree of melting and the generation of harzburgitic residues are expected to occur at the top of the mantle, whereas lherzolites are likely to be stable at greater depths (Becker and Dale, 2016). SAO and NJO whole-rock, orthopyroxene and olivine

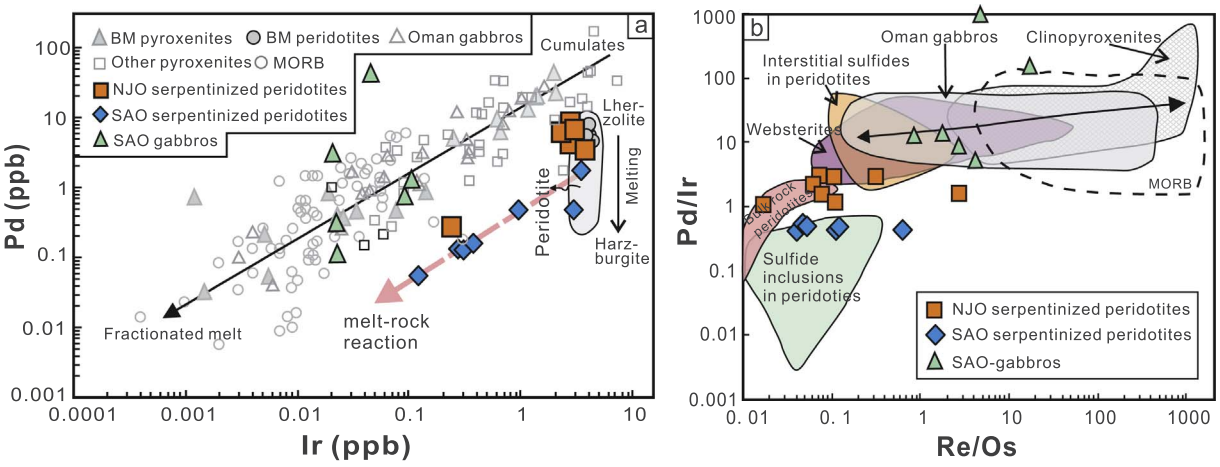

Fig. 12. Pd–Ir (a) and Pd/Ir–Re/Os (b) diagrams showing the PGE distributions of the SAO and NJO samples. The diagrams are re-drawn from Becker and Dale (2016).

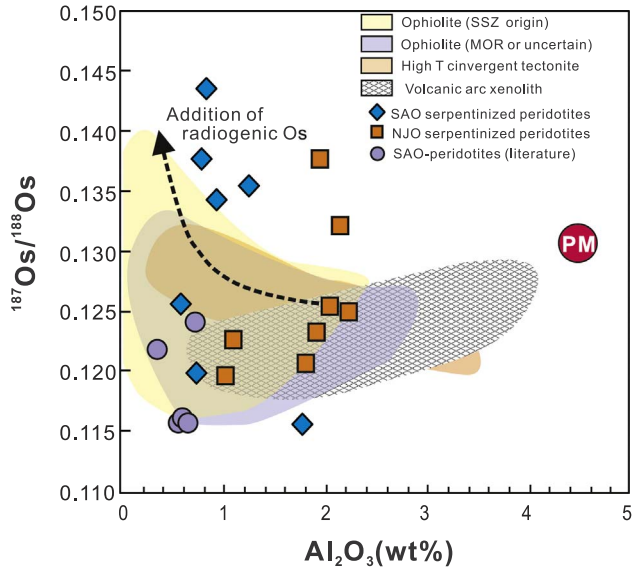

Fig. 13. $^{187}Os/^{188}Os$–Al_2O_3 diagram for the NJO and SAO serpentinized peridotites (modified after Becker and Dale, 2016). SAO peridotite data are from Ding (2008).

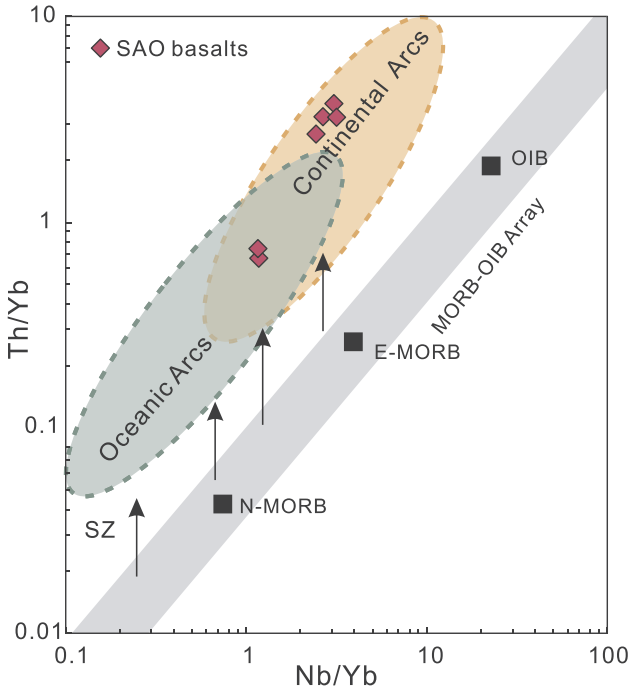

Fig. 14. Nb/Yb–Th/Yb diagram for the SAO basalts (modified after Pearce, 2014).

fragment compositions indicate that many of the samples were derived from harzburgitic protoliths, with only a few derived from dunites. This suggests that the SAO and NJO peridotites did not form in an ultra-slow-spreading setting. Furthermore, the SAO contains more gabbro and pyroxenite units than the NJO, indicating a relatively high spreading rate.

The differences in mantle characteristics between the SAO and NJO are also supported by the compositions of mafic rocks associated with the peridotites. SAO basalts and gabbros yield diverse REE patterns ranging from N-MORB- to typical IAB-like trends (Fig. 7). The basalts are enriched in Rb, U, Th, Ba, and K, and depleted in Nb, Ta, Zr, and Ti on the spidergrams (Fig. 8), consistent with a subduction zone setting. Th/Nb ratios can also be used to provide insights into the tectonic setting of magmatism, as Th is more mobile than Nb in subduction-related fluids, and rutile fractionation decreases Nb concentrations in the residual melt. Therefore, melts with high Th/Nb ratios are attributed to SSZ-type settings (Pearce, 2014). In a Th/Yb–Nb/Yb diagram, the SAO high-Al basalts plot within the continental arc field, whereas the low-Al basalts plot at the intersection between the continental and oceanic arc fields (Fig. 14). Moreover, the highly variable Rb, Ba, Th, U, K, and Sr concentrations in SAO gabbros and basalts are indicative of previous metasomatism by fluids released from subducted slabs.

The differences in mantle characteristics between the SAO and NJO can also be investigated through the interpretation of mineral compositions. SAO samples contain higher-Mg# olivine (mean = 91.7) and orthopyroxene (mean = 92.1) than the NJO (olivine mean = 89.5; orthopyroxene mean = 91.1). A high degree of melt extraction may generate residual olivine and orthopyroxene with elevated Mg# values. Spinel compositions can also be used to determine protoliths and constrain the degree of partial melting recorded by peridotites (Bonatti and Michael, 1989; Gao et al., 2015; Jaques and Green, 1980; Zhou et al., 1992). Dick and Bullen (1984) indicated that chromium is more compatible than aluminum, leading to a significant fractionation of these elements during partial melting. Therefore, higher degrees of partial melting will generate spinels with higher Cr# values. Chrome-spinel from the SAO complex has an average Cr# value of > 60 (Ding et al., 2008; Zhou et al., 1992), which is higher than that of the NJO complex (53.7; Zhou et al., 1992). Therefore, the SAO mantle peridotites likely underwent a higher degree of partial melting than did the NJO samples. Furthermore, melt infiltration and melt-peridotite reactions have been suggested to be critical processes during the formation of mantle tectonites in various tectonic settings (e.g., the Pyrenees, Ronda, Ligurides, Ivrea Zone, Lanzo, Horoman mantle tectonites, as well as abyssal peridotites and ophiolites) (Lorand et al., 2009). Convergent margin ophiolites generally contain many podiform chromitite units that are enveloped by dunite. The formation of these units in the SAO requires a high degree of melt extraction and likely significant melt-rock reaction. The above observations therefore indicate that the SAO peridotites formed in an active continental margin setting.

5.4. Implications for the convergence history on the eastern margin of the Yangtze Block

The tectonic setting of the SAO and NJO complexes has been debated for decades (Ding et al., 2008; Gao et al., 2009; Li et al., 1994, 1997, 2003; Wang et al., 2011; Wu et al., 2005; Xing, 1990; Xing et al., 1992; Zhang et al., 2012; Zhang et al., 2013; Zhao et al., 1995; Zhou et al., 1989). It is widely accepted that both ophiolites formed during Neoproterozoic subduction of oceanic crust during the amalgamation of the Yangtze and Cathaysia blocks (Charvet et al., 1996; Chen et al., 1991; Li et al., 1997, 2003, 2013a; Shu et al., 1995; Wang et al., 2004, 2007, 2012, 2013, 2014; Wu, 2007; Xu and Zhou, 1992; Zhang et al., 2012, 2013; Zhou and Zhu, 1993). However, their specific tectonic settings and roles in the amalgamation remain uncertain. For example, several different settings have been proposed for the SAO complex, including a back-arc basin associated with an intra-continental rift (Zhou et al., 1989), an island arc (Xing, 1990), and an extensional back-arc basin within a continental (i.e., Yangtze Block) marginal setting (Li et al., 2013b; Wu et al., 2005; Zhang et al., 2012). In addition, the slate, phyllite, and siltstone–sandstone units of the associated Shuangqiaoshan Group are consistent with a back-arc environment (e.g., Wang et al., 2014). As the SAO complex yields relatively high εNd(t) values (+4.4 to +5.5; Wang et al., 2011; Xing et al., 1992), previous workers have suggested a range of possible tectonic settings. These include a paleo-island arc (Xing et al., 1992), a back-arc extensional environment (Zhao et al., 1995), ridge subduction (Zhang et al., 2013), and the initial rifting phase of an intra-oceanic back-arc basin (Wang et al., 2015). It should also be noted that the NJO is roughly contemporaneous with the early phase of Shuangxiwu arc volcanism in NW Zhejiang (ca. 970–855 Ma; Wang et al., 2013), possibly indicating that the NJO

formed during early oceanic subduction along the southeastern margin of the Yangtze Block.

The combinations of Os isotopes and PGEs geochemistry were also helpful to understand the tectonic settings of the two ophiolite suites. As discussed above, the SAO peridotites record greater melt extraction than those from the NJO, as evidenced by their low trace element and PGE concentrations, Pd/Ir ratios, and Os isotopes. The SAO gabbros and pyroxenites yield variable initial $^{187}Os/^{188}Os$ values (Fig. 10), suggesting the incorporation of crustal materials. This inference is consistent with the trace element and whole-rock Nd isotopic compositions of basaltic rocks within the SAO (Li et al., 1997). Mantle peridotites in back-arc basin settings are apt to be metasomatized by fluid/melt related to subducted slabs, and often interact with continental-margin-derived crustal material. In contrast, fore-arc peridotites rarely record interaction with silicate melts and are unlikely to undergo extensive melting owing to a lack of fluid. Therefore, fore-arc peridotites usually preserve primitive Os and PGE characteristics, as is the case for most of the NJO samples.

It's worth pointing out that the two ophiolite suites are located in distinct tectonic locations. The NJO complex lies between the Cathaysia and southeast Yangtze blocks, whereas the SAO is located between the Shuangxiwu arc terrane and the Yangtze Block. Both ophiolite suites are associated with folded sedimentary sequences that yield maximum depositional ages of ca. 860–825 Ma (Wang et al., 2014), suggesting that neither ophiolite was emplaced before 860 Ma. Shu and Charvet (1996) reported a K–Ar age of 866 ± 14 Ma for rare blueschists within the NJO, inferring that they formed during deep subduction. This age is consistent with the age of obduction-related granites within the NJO (Li et al., 2008), but is earlier than the formation age of the folded basement strata in the region, suggesting that the NJO underwent two stages of tectonic emplacement. The first stage may have been related to slab roll-back in an early ocean–continent subduction zone in a fore-arc setting. In contrast, the second stage is consistent with tectonic emplacement of the SAO during the closure of back-arc basins along the margin of the Jiangnan Orogen.

The above observations, combined with new zircon U–Pb dating results, indicate that the NJO mantle peridotites formed during an early stage of convergence (ca. 1.0–0.9 Ga), during oceanic subduction and extensive oceanic arc magmatism. In contrast, SAO mantle peridotites formed at 831 ± 5 Ma as a result of extensive back-arc extension along the Jiangnan Orogen associated with the development of back-arc basalts (Zhang et al., 2017). Back-arc extension was likely located proximal to the continental arc and was rapid enough to promote significant mantle metasomatism and melting. During later orogenesis and closure of the back-arc basins, the mantle peridotites were exhumed and tectonically emplaced into the metasedimentary Shangxi Group or Shuangqiaoshan Group sequences.

6. Conclusions

SHRIMP zircon U–Pb data indicate that the South Anhui ophiolite formed at 831 ± 5 Ma. Whole-rock geochemistry, PGE concentrations, and Os isotopic compositions, as well as EMPA analyses of relict olivine and orthopyroxene grains, suggest that the mantles of the SAO and NJO are distinct. However, both complexes contain serpentinized harzburgite-derived peridotites. Compared with those from the NJO, SAO peridotites are more depleted in trace elements, fractionated in PGE, and have more variable Os isotopic compositions. All of these lines of evidence suggest that the mantle sources of the SAO have experienced greater melt extraction than the peridotites within the NJO.

Combined studies on field, geochemistry, Re–Os isotopes and PGE data indicate that the SAO and NJO represent SSZ-type ophiolites. The NJO complex likely formed in a fore-arc setting in the late Mesoproterozoic to early Neoproterozoic, whereas the SAO complex formed in a back-arc extensional setting in the middle Neoproterozoic. The formations of these ophiolites record orogenic processes from the subduction of oceanic crust (early stage) to back-arc extension (late stage) and finally the closure of back-arc basins.

Acknowledgements

This work was financially supported by the State Key R&D Program of China (2016YFC0600203), the National Natural Science Foundation of China (41330208 and 41222016), and the Program for New Century Excellent Talents in University of China (NCET, to X.L. Wang). The manuscript benefited greatly from the critical and thoughtful comments of five anonymous reviewers and the editor, Prof. S.B. Zhang. We thank B. Wu for LA–ICP–MS dating, and W.L. Xie and J.F. Gao for major and trace element analyses, respectively.

Appendix A. Supplementary data

Supplementary data associated with this article can be found, in the online version, at http://dx.doi.org/10.1016/j.precamres.2017.12.042.

References

Alard, O., Griffin, W.L., Lorand, J.P., Jackson, S.E., O'Reilly, S.Y., 2000. Non-chondritic distribution of the highly siderophile elements in mantle sulphides. Nature 407, 891–894.

Alard, O., Griffin, W.L., Pearson, N.J., Lorand, J.P., O'Reilly, S.Y., 2002. New insights into the Re-Os systematics of sub-continental lithospheric mantle from in situ analysis of sulphides. Earth Planet. Sci. Lett. 203, 651–663.

Bai, W.J., Gan, Q.G., Yang, J.S., Xing, F.G., Xu, X., 1986. Discovery of Well-reserved ophiolite and its basical characters in southeastern margin of the Jiangnan ancient continent. Acta Petrol. Mineral. 5, 289–299 (in Chinese with English abstract).

Ballhaus, C., Bockrath, C., Wohlgemuth-Ueberwasser, C., Laurenz, V., Berndt, J., 2006. Fractionation of the noble metals by physical processes. Contrib. Mineral. Petrol. 152, 667–684.

Barnes, S., Naldrett, A.J., Gorton, M.P., 1985. The origin of the fractionation of platinum-group elements in terrestrial magmas. Chem. Geol. 53, 303–323.

Batanova, V.G., Brügmann, G.E., Bazylev, B.A., Sobolev, A.V., Kamenetsky, V.S., Hofmann, A.W., 2008. Platinum-group element abundances and Os isotope composition of mantle peridotites from the Mamonia Complex. Cyprus. Chem. Geol. 248, 195–212.

Becker, H., Dale, C.W., 2016. Re–Pt–Os Isotopic and highly siderophile element behavior in oceanic and continental mantle tectonites. Rev. Mineral. Geochem. 81, 369–440.

Bjerg, S.C.D., Mogessie, A., Bjerg, E., 1995. PASFORM: a program for IBM PC or PC-compatible computers to calculate mineral formulae from electron microprobe and wet-chemical analysis. Pergamon Press Inc.

Black, L.P., Kamo, S.L., Williams, I.S., Mundil, R., Davis, D.W., Korsch, R.J., Foudoulis, C., 2003. The application of SHRIMP to Phanerozoic geochronology: a critical appraisal of four zircon standards. Chem. Geol. 200, 171–188.

Black, L.P., Kamo, S.L., Allen, C.M., Davis, D.W., Aleinikoff, J.N., Valley, J.W., Mundil, R., Campbell, L.H., Korsch, R.J., Williams, I.S., Foudoulis, C., 2004. Improved $^{206}Pb/^{238}U$ microprobe geochronology by the monitoring of a trace-element-related matrix effect: SHRIMP, IT–TIMS, ELA–ICP–MS and oxygen isotope documentation for a series of zircon standards. Chem. Geol. 205, 115–140.

Bockrath, C., Ballhaus, C., Holzheid, A., 2004. Fractionation of the platinum-group elements during mantle melting. Science 305, 1951–1953.

Bonatti, E., Michael, P.J., 1989. Mantle peridotites from continental rifts to ocean basins to subduction zones. Earth Planet. Sci. Lett. 91, 297–311.

Boudier, F., Godard, M., Armbruster, C., 2000. Significance of gabbronorite occurrence in the crustal section of the Semail ophiolite. Marine Geophys. Res. 21, 307–326.

Brandon, A.D., Snow, J.E., Walker, R.J., Morgan, J.W., 2000. $^{190}Pt^{186}Os$ and $^{187}Re–^{187}Os$ systematics of abyssal peridotites. Earth Planet. Sci. Lett. 177, 319–335.

Büchl, A., Brügmann, G., Batanova, V.G., Münker, C., Hofmann, A.W., 2002. Melt percolation monitored by Os isotopes and HSE abundances: a case study from the mantle section of the Troodos Ophiolite. Earth Planet. Sci. Lett. 204, 385–402.

Charvet, J., Shu, L., Shi, Y., Guo, L., Faure, M., 1996. The building of south China: collision of Yangzi and Cathaysia blocks, problems and tentative answers. J. Asian Earth Sci. 13, 223–235.

Chen, J.F., Foland, K.A., Xing, F.M., Xu, X., Zhou, T.X., 1991. Magmatism along the southeast margin of the Yangtze block: Precambrian collision of the Yangtze and Cathysia blocks of China. Geology 19, 815–818.

Dewey, J.F., Bird, J.M., 1971. Origin and emplacement of the ophiolite suite: Appalachian ophiolites in Newfoundland. J. Geophys. Res. 76, 3179–3206.

Dick, H.J.B., Bullen, T., 1984. Chromian spinel as a petrogenetic indicator in abyssal and alpine-type peridotites and spatially associated lavas. Contrib. Miner. Petrol. 86 (1), 54–76.

Dilek, Y., Furnes, H., 2011. Ophiolite genesis and global tectonics: geochemical and tectonic fingerprinting of ancient oceanic lithosphere. GSA Bull. 123, 387–411.

Ding, B.H., 2008. Re-Os isotopic geochemistry of the SSZ-type ophiolites in South Anhui Province. Master's thesis of University of Science and Technology of China, pp. 1–88 (in Chinese with English abstract).

Ding, B.H., Shi, R.D., Zhi, X.C., Zheng, L., Chen, L., 2008. Neoproterozoic (~850 Ma) subduction in the Jiangnan orogen: evidence from the SHRIMP U-Pb dating of the SSZ-type ophiolite in southern Anhui Province. Acta Petrol. Mineral. 27, 375–388 (in Chinese with English abstract).
Gao, J., Klemd, R., Long, L.L., Xiong, X.M., Qian, Q., 2009. Adakitic signature formed by fractional crystallization: An interpretation for the Neo-Proterozoic meta-plagio-granites of the NE Jiangxi ophiolitic mélange belt, South China. Lithos 110, 277–293.
Gao, J.F., Zhou, M.F., Leung, H.S.S., Robinson, P.T., Yang, S.H., 2015. Re–Os isotopic and platinum group elemental constraints on the genesis of the Xiadong ophiolitic complex, Eastern Xinjiang, NW China. Gondwana Res. 27, 629–648.
Gao, S., Rudnick, R.L., Carlson, R.W., McDonough, W.F., Liu, Y.-S., 2002. Re–Os evidence for replacement of ancient mantle lithosphere beneath the North China craton. Earth Planet. Sci. Lett. 198, 307–322.
Garuti, G., Oddone, M., Torresruiz, J., 1997. Platinum-group-element distribution in subcontinental mantle: evidence. Canad. J. Earth Sci. 34, 444–483.
Handler, M.R., Bennett, V.C., Esat, T.M., 1997. The persistence of off-cratonic lithospheric mantle: Os isotopic systematics of variably metasomatised southeast Australian xenoliths. Earth Planet. Sci. Lett. 151, 61–75.
Hébert, R., Bezard, R., Guilmette, C., Dostal, J., Wang, C.S., Liu, Z.F., 2012. The Indus-Yarlung Zangbo ophiolites from Nanga Parbat to Namche Barwa syntaxes, southern Tibet: First synthesis of petrology, geochemistry, and geochronology with incidences on geodynamic reconstructions of Neo-Tethys. Gondwana Res. 22, 377–397.
Ishikawa, T., Nagaishi, K., Umino, S., 2002. Boninitic volcanism in the Oman ophiolite: Implications for thermal condition during transition from spreading ridge to arc. Geology 30, 899–902.
Jaques, A.L., Green, D.H., 1980. Anhydrous melting of peridotite at 0–15 Kb pressure and the genesis of tholeiitic basalts. Contrib. Mineral. Petrol. 73 (3), 287–310.
Kelemen, P.B., Yogodzinski, G.M., Scholl, D.W., 2003. Along-strike variation in the Aleutian Island Arc: Genesis of high Mg# andesite and implications for continental crust. Washington Dc American Geophys. Union Geophys. Monograph 138 (1), 223–276.
Lambert, D.D., Foster, J.G., Frick, L.R., Ripley, E.M., Zientek, M.L., 1998. Geodynamics of magmatic Cu-Ni-PGE sulfide deposits: new insights from the Re-Os isotope system. Econ. Geol. 93 (2), 121–136.
Li, L.M., Lin, S.F., Xing, G.F., Davis, D.W., Davis, W.J., Xiao, W.J., Yin, C.Q., 2013b. Geochemistry and tectonic implications of late Mesoproterozoic alkaline bimodal volcanic rocks from the Tieshajie Group in the southeastern Yangtze block, south China. Precambrian Res. 230 (2), 179–192.
Li, L.M., Lin, S.F., Xing, G.F., Davis, D.W., Davis, W.J., Xiao, W.J., Yin, C.Q., 2013a. Geochronology and geochemistry of volcanic rocks from the Shaojiwa Formation and Xingzi Group, Lushan area, se China: implications for Neoproterozoic back-arc basin in the Yangtze block. Precambrian Res. 238, 1–17.
Li, W.X., Li, X.H., Li, Z.X., Lou, F.S., 2008. Obduction-type granites within the NE Jiangxi Ophiolite: Implications for the final amalgamation between the Yangtze and Cathaysia Blocks. Gondwana Res. 13, 288–301.
Li, X.H., Zhou, G.Q., Zhao, J.X., Fanning, C.M., Compston, w., 1994. SHRIMP ion microprobe zircon U-Pb age of the NE Jiangxi Ophiolite and its tectonic implications. Geochimica 2, 125–131 (in Chinese with English Abstract).
Li, X.H., Zhao, J.X., McCulloch, T.M., Zhou, G.Q., Xing, F.M., 1997. Geochemical and Sm-Nd isotopic study of Neoproterozoic ophiolites from southeastern China: petrogenesis and tectonic implications. Precambrian Res. 81, 129–144.
Li, X.H., Li, Z.X., Ge, W.C., Zhou, H.W., Li, W.X., Liu, Y., Wingate, M.T.D., 2003. Neoproterozoic granitoids in South China: crustal melting above a mantle plume at ca. 825Ma? Precambrian Res. 122, 45–83.
Li, Y., Xie, H.Q., Song, Z.R., 2017. SHRIMP U-Pb zircon ages of the northeastern Jiangxi ophiolites and the Zhangcun Group and a discussion on the tectonic evolution of the Jiangnan Orogen. Geol. Rev. 63, 855–868 (in Chinese with English abstract).
Lister, G., Forster, M., 2009. Tectonic mode switches and the nature of orogenesis. Lithos 113, 274–291.
Lorand, J.P., Alard, O., Godard, M., 2009. Platinum-group element signature of the primitive mantle rejuvenated by melt-rock reactions: evidence from Sumail peridotites (Oman Ophiolite). Terra Nova 21, 35–40.
Luguet, A., Lorand, J.P., Seyler, M., 2003. A coupled study of sulfide petrology and highly siderophile element geochemistry in abyssal peridotites from the Kane Fracture Zone (45°W 23°20′N, MARK area, Atlantic Ocean). Geochim. Cosmochim. Acta 67, 1553–1570.
McDonough, W.F., Sun, S.S., 1995. Composition of the Earth. Geochim. Geol. 120, 223–253.
Meisel, T., Walker, R.J., Morgan, J.W., 1996. The Osmium isotopic composition of the Earth's primitive upper mantle. Nature 383, 517–520.
Meisel, T., Moser, J., 2004. Reference materials for geochemical PGE analysis: New analytical data for Ru, Rh, Pd, Os, Ir, Pt and Re by isotope dilution ICP-MS in 11 geological reference materials. Chem. Geol. 208, 319–338.
Mitchell, R.H., Keays, R.R., 1981. Abundance and distribution of gold, palladium and iridium in some spinel and garnet lherzolites — implications for the nature and origin of precious metal-rich intergranular components in the upper mantle. Geochim. Cosmochim. Acta 45, 2425–2442.
Moores, E.M., Robinson, P.T., Malpas, J., Xenophonotos, C., 1984. Model for the origin of the Troodos massif, Cyprus, and other Mideast ophiolites. Geology 12, 500–503.
Morris, A., Anderson, M.W., Robertson, A.H.F., Al-Riyami, K., 2002. Extreme tectonic rotations within an eastern Mediterranean ophiolite (Baër–bassit, Syria). Earth Planet. Sci. Lett. 202, 247–261.
Nicolas, A., 1989. Structures of Ophiolites and Dynamics of Oceanic Lithosphere. Structures of Ophiolites and Dynamics of Oceanic Lithosphere. Kluwer Academic Publishers.
Pearce, J.A., 2014. Immobile element fingerprinting of ophiolites. Elements 10, 101–108.
Peslier, A.H., Reisberg, L., Ludden, J., Francis, D., 2000. Re–Os constraints on harzburgite and lherzolite formation in the lithospheric mantle: A study of Northern Canadian Cordillera xenoliths. Geochim. Cosmochim. Acta 64, 3061–3071.
Qi, L., Hu, J., Conrad Gregoire, D., 2000. Determination of trace elements in granites by inductively coupled plasma mass spectrometry. Talanta 51, 507–513.
Qi, L., Gao, J.F., Zhou, M.F., Hu, J., 2013. The design of re-usable carius tubes for the determination of rhenium, osmium and platinum-group elements in geological samples. Geostand. Geoanaly. Res. 37, 345–351.
Qi, L., Zhou, M.F., Wang, C.Y., 2004. Determination of low concentrations of platinum group elements in geological samples by ID-ICP-MS. J. Analy. Atomic Spectr. 19, 1335–1339.
Qi, L., Zhou, M.F., Wang, C.Y., Sun, M., 2007. Evaluation of a technique for determining Re and PGEs in geological samples by ICP-MS coupled with a modified Carius tube digestion. Geochem. J. 41, 407–414.
Rehkämper, M., Halliday, A.N., Fitton, J.G., Lee, D.C., Wieneke, M., Arndt, N.T., 1999. Ir, Ru, Pt and Pd in basalts and komatiites: New constraints for the geochemical behavior of the Platinum-group elements in the mantle. Geochim. Cosmochim. Acta 63, 3915–3934.
Reisberg, L., Lorand, J.P., 1995. Longevity of sub-continental mantle lithosphere from osmium isotope systematics in orogenic peridotite massifs. Nature 376, 159–162.
Santosh, M., Liu, S.J., Tsunogae, T., Li, J.H., 2012. Paleoproterozoic ultrahigh-temperature granulites in the North China Craton: Implications for tectonic models on extreme crustal metamorphism. Precambrian Res. 222–223, 77–106.
Santosh, M., Shaji, E., Tsunogae, T., Mohan, M.R., Satyanarayanan, M., Horie, K., 2013. Suprasubduction zone ophiolite from Agali hill: Petrology, zircon SHRIMP U-Pb geochronology, geochemistry and implications for Neoarchean plate tectonics in southern India. Precambrian Res. 231, 301–324.
Shu, L.S., Zhou, G.Q., Shi, Y.S., Yin, J., 1993. Study of high pressure metamorphic blueschist and its late Proterozoic age in the eastern Jiangnan belt. Chin. Sci. Bull. 38, 779–882 (in Chinese).
Shu, L.S., Shi, Y.S., Gou, L.Z., Charvet, J., Sun, Y. (Eds.), 1995. Plate tectonic evolution and the kinematics of collisional orogeny in the Middle Jiangnan, eastern China. Nanjing University Publ. (in Chinese with English abstract).
Shu, L.S., Charvet, J., 1996. Kinematics and geochronology of the Proterozoic Dongxiang-Shexian ductile shear zone: with HP metamorphism and ophiolitic mélange (Jiangnan region, South China). Tectonophysics 267, 291–302.
Snow, J., Reisberg, L., 1995. Os isotopic systematics of the MORB mantle: results from altered abyssal peridotites. Earth Planet. Sci. Lett. 133, 411–421.
Snow, J.E., Schmidt, G., 1998. Constraints on Earth accretion deduced from noble metals in the oceanic mantle. Nature 391, 166–169.
Sun, S.S., McDonough, W.F., 1989. Chemical and isotopic systematics of oceanic basalt: Implications for mantle composition and processes, *in* Magmatism in the ocean basins. In: Saunders, A.D., Norry, M.J. (Eds.), 42. Spec. Publ. Geol. Soc., London, pp. 528–548.
Taylor, S.R., Mclennan, S.M., 1995. The geochemical evolution of the continental crust. Rev. Geophy. 33, 293–301.
Valley, J.W., Kinny, P.D., Schulze, D.J., Spicuzza, M.J., 1998. Zircon megacrysts from kimberlite: oxygen isotope variability among mantle melts. Contrib. Mineral. Petrol. 133, 1–11.
Walker, R.J., Horan, M.F., Morgan, J.W., Becker, H., Grossman, J.N., Rubin, A.E., 2002. Comparative ^{187}Re-^{187}Os systematics of chondrites: Implications regarding early solar system processes. Geochim. Cosmochim. Acta. 66, 4187–4201.
Wan, Y.S., Zhang, Y., Williams, I.S., Liu, D., Dong, C., Fan, R., Shi, R., Ma, M.Z., 2013. Extreme zircon O isotopic compositions from 3.8 to 2.5Ga magmatic rocks from the Anshan area. North China Craton. Chem. Geol. 352, 108–124.
Wang, C.Z., Huang, Z.Z., Xing, G.F., Yu, M.G., Hong, W.T., 2016. The origin of the mantle peridotite from ophiolite in northeast Jiangxi and its geological implications. Geol. China 43, 1178–1188 (in Chinese with English abstract).
Wang, C.Z., Jiang, Y., Xing, G.F., 2011. Recent situation of researches on ophiolites and some problems concerning the ophiolites in south China. Resour. Surv. Environ. 32 (4), 235–246 (in Chinese with English abstract).
Wang, L.J., Griffin, W.L., Yu, J.H., O'Reilly, S.Y., et al., 2010. Precambrian crustal evolution of the Yangtze Block tracked by detrital zircons from Neoproterozoic sedimentary rocks. Precambrian Res. 177, 131–144.
Wang, X.L., Zhou, J.C., Qiu, J.S., Gao, J.F., 2004. Geochemistry of the Meso- to Neoproterozoic basic-acid rocks from Hunan Province, South China: implications for the evolution of the western Jiangnan orogen. Precambrian Res. 135, 79–103.
Wang, X.L., Zhou, J.C., Griffin, W.L., Wang, R.C., Qiu, J.S., O'Reilly, S.Y., Xu, X.S., Liu, X.M., Zhang, G.L., 2007. Detrital zircon geochronology of Precambrian basement sequences in the Jiangnan orogen: dating the assembly of the Yangtze and Cathaysia blocks. Precambrian Res. 159, 117–131.
Wang, X.L., Shu, L.S., Xing, G.F., Zhou, J.C., Tang, M., Shu, X.J., Qi, L., Hu, Y.H., 2012. Post-orogenic extension in the eastern part of the Jiangnan orogen: evidence from ca 800–760 Ma volcanic rocks. Precambrian Res. 222–223, 404–423.
Wang, X.L., Zhou, J.C., Wan, Y.S., Kitajima, K., Wang, D., Bonamici, C., Qiu, J.S., Sun, T., 2013. Magmatic evolution and crustal recycling for Neoproterozoic strongly peraluminous granitoids from southern China: Hf and O isotopes in zircon. Earth Planet. Sci. Lett. 366, 71–82.
Wang, X.L., Zhou, J.C., Griffin, W.L., Zhao, G.C., Yu, J.H., Qiu, J.S., Zhang, Y.J., Xing, G.F., 2014. Geochemical zonation across a Neoproterozoic orogenic belt: Isotopic evidence from granitoids and metasedimentary rocks of the Jiangnan orogen, China. Precambrian Res. 242, 154–171.
Wang, C.Z., Xing, G.F., Yu, M.G., Huang, Z.Z., Hong, W.T., Zhao, X.L., Zhou, X.H., Duan, Z., Ju, D.M., 2015. Timing and tectonic setting of the ophiolite in northeast Jiangxi: Constrains from zircon U-Pb age, Hf isotope and geochemistry of the Zhangshudun gabbro. Acta Petrol. Mineral. 34 (3), 309–321 (in Chinese with English abstract).

Williams, I.S., 1998. U-Th-Pb geochronology by ion microprobe. Rev. Econ. Geol. 7, 1–35.
Wu, X.H., 2007. Rediscuss of Shuangqiaoshan Group. Resour. Surv. Environ. 28, 95–105 (in Chinese with English Abstract).
Wu, R.X., Zheng, Y.F., Wu, Y.B., 2005. Zircon U-Pb age, element and oxygen isotope geochemisty of Neoproterozoic granodiorites in South Anhui. Acta Petrol. Sin. 21 (3), 587–606 (in Chinese with English Abstract).
Xing, F.M., 1990. Geochemical indication of formation environment of fuchuan ophiolites in southern Anhui Province. Acta Petrol. Mineral. 9, 1–12 (in Chinese with English abstract).
Xing, F.M., Xu, X., Chen, J.F., Zhou, T.X., Foland, K.A., 1992. The late Proterozoic continental accretionary history of the southeastern margin of the Yangtze platform. Acta Geol. Sin. 66, 59–71 (in Chinese with English abstract).
Xu, X.S., Zhou, X.M., 1992. Precambrian S-type granitoids in South China and their geological significance. J. Nanjing Univ. (Nat. Sci. Ed.) 28, 423–430 (in Chinese with English abstract).
Xue, H.M., Ma, F., Song, Y.Q., Xie, Y.P., 2010. Geochronology and geochemistry of the Neoproterozoic granitoid association from eastern segment of the Jiangnan orogen, China: Constraints on the timing and process of amalgamation between the Yangtze and Cathaysia blocks. Acta Petrol. Sin. 26 (11), 3215–3244 (in Chinese with English abstract).
Yin, C.Q., Lin, S.F., Davis, D.W., Xing, G.F., Davis, W.J., Cheng, G.H., Xiao, W.J., Li, L.M., 2013. Tectonic evolution of the southeastern margin of the Yangtze block: constraints from shrimp U-Pb and LA-ICP-MS Hf isotopic studies of zircon from the eastern Jiangnan orogenic belt and implications for the tectonic interpretation of South China. Precambrian Res. 236, 145–156.
Zhang, C., Li, H., Santosh, M., 2013. Revisiting the tectonic evolution of South China: interaction between the Rodinia superplume and plate subduction? Terra Nova 25 212–220.
Zhang, C.L., Santosh, M., Zou, H.B., Li, H.K., Huang, W.C., 2013. The Fuchuan ophiolite in Jiangnan Orogen: Geochemistry, zircon U-Pb geochronology, Hf isotope and implications for the Neoproterozoic assembly of South China. Lithos 179, 263–274.
Zhang, C.L., Zou, H.B., Zhu, Q.B., Chen, X.Y., 2015. Late Mesoproterozoic to early Neoproterozoic ridge subduction along southern margin of the Jiangnan Orogen: New evidence from the Northeastern Jiangxi Ophiolite (NJO), South China. Precambrian Res. 268, 1–15.
Zhang, F.F., Wang, X.L., Wang, D., Yu, J.H., Zhou, X.H., Sun, Z.M., 2017. Neoproterozoic backarc basin on the southeastern margin of the Yangtze block during Rodinia assembly: New evidence from provenance of detrital zircons and geochemistry of mafic rocks. GSA Bull. 129http://dx.doi.org/10.1130/B31528.1. (in press).
Zhang, S.B., Wu, R.X., Zheng, Y.F., 2012. Neoproterozoic continental accretion in South China: Geochemical evidence from the Fuchuan ophiolite in the Jiangnan orogen. Precambrian Res. 220–221, 45–64.
Zhang, S.B., Zheng, Y.F., 2013. Formation and evolution of Precambrian continental lithosphere in South China. Gondwana Res. 23, 1241–1260.
Zhao, G.C., Cawood, P.A., 1999. Tectonothermal evolution of the Mayuan Assemblage in the Cathaysia Block: implications for Neoproterozoic collision-related assembly of the South China Craton. Am. J. Sci. 299, 309–339.
Zhao, G.C., Cawood, P.A., 2012. Precambrian geology of China. Precambrian Res. 222–223, 13–54.
Zhao, J., Li, X., Mcculloch, M.T., Zhou, G., Xing, F., 1995. Petrogenesis of ophiolites from south Anhui and northeast Jiangxi, and their tectonic implications: chemical and Sm-Nd isotopic constraints. Geochimica 24, 311–326 (in Chinese with English abstract).
Zheng, Y.F., Wu, R.X., Wu, Y.B., Zhang, S.B., Yuan, H., Wu, F.Y., 2008. Rift melting of juvenile arc-derived crust: geochemical evidence from Neoproterozoic volcanic and granitic rocks in the Jiangnan Orogen, South China. Precambrian Res. 163, 351–383.
Zhou, G.Q., Zhao, J.X., 1991. Sm-Nd isotope study of Ophiolite in Northeastern Jiangxi in the Southeastern margin of Yangtze Craton, South China. Chin. Sci. Bull. 2, 129–132 (in Chinese).
Zhou, J.C., Wang, X.L., Qiu, J.S., Gao, J.F., 2004. Geochemistry of Meso- and Neoproterozoic mafic- ultramafic rocks from northern Guangxi, China: arc or plume magmatism? Geochem. J. 38, 139–152.
Zhou, J.Y., 2013. Mineral rock type study of Ophiolite suite in Southern Anhui. Sci. Technol. Inform. 24, 462–463 (in Chinese).
Zhou, X.M., Wang, D.Z., 1988. The peraluminous granodiorites with low initial $^{87}Sr/^{86}Sr$ ratio and their genesis in southern Anhui Province, eastern China. Acta Petrol. Sin. 4, 37–45 (in Chinese with English abstract).
Zhou, X.M., Zou, H.B., Yang, J.D., Wang, Y.X., 1989. Sm-Nd isochron age and geological significance of Fuchuan ophiolite suite in Shexian, Anhui. Chin. Sci. Bull. 16, 1243–1245 (in Chinese).
Zhou, X.M., Yu, J.H., Xu, X.S., 1992. Discovery and significance of granulite xenoliths in Nushan basalt, East China. Chin. Sci. Bull. 37, 1730–1734 (in Chinese).
Zhou, X.M., Zhu, Y.H., 1993. Petrological evidence for a Late Proterozoic collisional orogenic belt and suture zone in southeast China. In: Li, J.L. (Ed.), The Structure and Geological Evolution of the Continental Lithosphere in Southeast China. Metallurgic Industry Press, Beijing, pp. 87–97 (in Chinese with English abstract).